

Design of an Antagonistically Counter-Balancing Parallel Mechanism

Jong-Tae Seo, Jae Hong Woo, Hoon Lim, Jaeheon Chung, Whee Kuk Kim, and Byung-Ju Yi,
Member, IEEE

Abstract— Much attention has not been paid to analysis of the open-loop stability for gravity counter-balancing of parallel mechanisms or closed-chain mechanisms. The open-loop stability is crucial especially in passively counter-balanced mechanisms where no actuators are involved. Passive hands-on device is such an example. A general stiffness model is derived for general closed-chain mechanism including counter-weight model. As a measure of the open-loop stability, we employ the determinant of the stiffness matrix. A parallel mechanism having 3 translational DOF (degree of freedom) is employed as an exemplary device. An antagonistically counter-balancing is found the most stable method. We conduct dynamic simulation and experiment to confirm the open-loop stability of the system.

I. INTRODUCTION

Counter-balancing mechanisms have been employed extensively in many different applications such as static balancing parts in automotive industry, gravity compensation for industrial robot, service robot, home furniture, medical devices, construction machines in heavy industry, and so on.

Especially in robot applications, the concept of counter-balancing mechanism has been widely employed to compensate for gravity load of links and resultantly increase the payload of the robot. There are two ways of counter-balancing; counter-weight and passive spring.

In the design of haptic mechanism, Laliberte and Gosselin [1] investigated counter-balancing of a 3-DOF planar parallel mechanism by attaching a counter-weight and spring at some links and joints. Wang and Gosselin [2, 3] designed 3-DOF and 6-DOF spatial parallel mechanisms in a similar manner. Tahmasebi, et al [4] designed a 5-bar parallel mechanism by using actuator as a counter-weight.

In the design of rehabilitation devices, Agrawal and Agrawal [5] designed a gravity-balancing auxiliary

parallelogram mechanism by using springs at some links and joints.

In the design of medical device, Nakamura, et al [6] designed a gravity-balancing serial mechanism using timing belt by attaching a counter-weight at the end point of the lower link. Nakamura, et al [7, 8] designed a gravity-balancing parallelogram mechanism by using an adjustable moment arm. Nakamura [9] designed a balancing chair for medical apparatus. Lessard, et al [10] designed a 5-bar gravity-balancing parallel mechanism by using torsion springs at joints. In the design of service robot, Park, et al. [11] designed a counter-balancing serial mechanism by attaching a spring at each joint.

Need for counter-balancing mechanism is expected to grow much specially in the area of smart hands-on devices. The medical microscope being used in operation room is such an example. Devising mechanisms handling a heavy load with less human power is also demanding at factory or warehouse.

Although there have been quite a few counter-balancing designs for several purposes, a little attention has been paid to analysis of the open-loop stability. As a matter of fact, analysis of the open-loop stability is significant in the design of passive hands-on devices, because such devices do not employ any motors as opposed to the feedback control scheme using actuators. It is noted that in a state of static equilibrium between weights of the hands-on device and the counter-weight, the system tends to oscillate like a spring once the system is perturbed from its equilibrium state. Yi and Freeman [12] analyzed the open-loop stability of a serial type manipulator when the manipulator maintained a contact with environment. Yi and Freeman [13] suggested a general stiffness model for redundantly actuated parallel mechanisms with which the open-loop stability was analyzed in part. However, there has not been any prior work that analyzes the open-loop stability when any robot mechanism is balanced by counter-weight or spring. Thus, in this paper we would like to generalize the stiffness model of parallel mechanisms for analysis of the open-loop stability.

This paper can be organized as follows. In section II, the kinematics is shortly described. Section III deals with the general stiffness model for parallel mechanisms by incorporating counter-weight model. In section IV, the open-loop stability is analyzed with one exemplary parallel mechanism having three degrees of freedom. As a result, an antagonistically counter-balancing is suggested as a sub-optimal design for ensuring open-loop stability. Furthermore, in order to ensure the open-loop stability and minimize the restoring force throughout the workspace, an

J. -T. Seo is with the Department of Mechatronics Engineering, Hanyang University, Ansan, Korea (e-mail: jt1000je@nate.com).

J. H. Woo is with the Department of Intelligent Robot Engineering, Hanyang University, Ansan, Korea (e-mail: jokers12@nate.com).

H. Lim is with the Department of Electronic, Electrical, Control and Instrumentation Engineering, Hanyang University, Ansan, Korea (e-mail: jokers12@nate.com and hoonlim78@gmail.com).

J. Chung is with the Koh Young Technology Inc., Seoul, Korea (e-mail: jaeheon.chung@gmail.com).

W. K. Kim is with Department of Control and Instrumentation Engineering, Korea University, Korea. (e-mail: wheekuk@korea.ac.kr).

B. -J. Yi is with the Department of Electronic Systems Engineering, Hanyang University, Ansan, Korea (corresponding author to provide phone: +82-31-400-5026; fax: +82-31-400-5027; e-mail: bj@hanyang.ac.kr).

adjustable moment arm is designed at joints where counter-weights are installed. Section V demonstrates the experimental result to show the feasibility of the proposed counter-balancing mechanism. Lastly, we draw conclusion.

II. KINEMATICS AND NOMENCLATURE

A. Kinematics Modeling

1. Open-chain kinematics

For a given open-chain manipulator, adopting the standard Jacobian $[G_\phi^u]$ representation for the velocity of a vector of P dependent (output) coordinates u in terms of a set M independent input coordinates ϕ , we have

$$\dot{u} = [G_\phi^u] \dot{\phi}. \quad (1)$$

To represent the second-order kinematics, a particular matrix formulation is chosen in which the non-linear, velocity related components are expressed in terms of a three-dimensional coefficient array $[H_{\phi\phi}^u]$, (note that it consists of purely configuration dependent second-order partial derivatives) [14]. Generally, the acceleration vector \ddot{u} of a set of P dependent coordinates u is represented in terms of the M independent coordinates ϕ as

$$\ddot{u} = [G_\phi^u] \ddot{\phi} + \dot{\phi}^T [H_{\phi\phi}^u] \dot{\phi}. \quad (2)$$

2. Closed-chain kinematics

Based on the previous open-chain kinematics, the following discusses the closed-chain kinematics of general closed-chain or parallel mechanisms. The kinematic modeling methodology for closed-chain systems is illustrated here in terms of R , M_r -DOF chains connected to a common object moving in an N -dimensional space (see Fig. 1). In general, each chain may have different degrees of freedom (M_r).

The first goal here is to obtain the closed-chain kinematic model (S_a^p) of general closed-chain mechanisms as follows

$$(S_a^p) = [G_a^p], [H_{aa}^p] \quad (3)$$

where $[G_a^p]$ and $[H_{aa}^p]$ denote the first- and second-order internal KIC relating the dependent coordinate set (expressed as ‘ p ’) to the independent coordinate set (minimum actuation set, expressed as ‘ a ’), respectively. This kinematic model will be useful to obtain the dynamic and stiffness models of general closed-chain mechanisms.

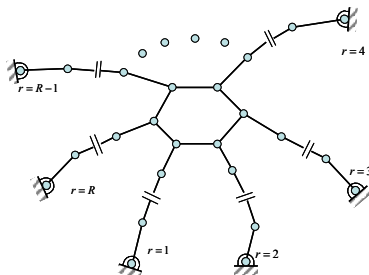


Figure 1. Closed-Chain Mechanism.

Then, the forward kinematics model (S_a^u) of general closed-chain mechanisms is given by

$$(S_a^u) = [G_a^u], [H_{aa}^u] \quad (4)$$

where $[G_a^u]$ and $[H_{aa}^u]$ denote the first- and second-order KIC relating the common object/end-effector coordinate set to the minimum actuation set, respectively.

2.1. Forward kinematics in higher-orders

Given the velocity and acceleration vector of a set of common coordinates, the open tree structure of a multi-chain mechanism yields the joint velocity and acceleration relations for the ‘ r ’ chains as follows;

$$\dot{u} = [{}_r G_\phi^u] {}_r \dot{\phi} \quad (5)$$

$$\ddot{u} = [{}_r G_\phi^u] {}_r \ddot{\phi} + {}_r \dot{\phi}^T [{}_r H_{\phi\phi}^u] {}_r \dot{\phi}, \quad (r=1, 2, 3, \dots, R) \quad (6)$$

Eq. (5) implies that for a common task space velocity vector \dot{u} , there are $(R-1)$ relations relating one of the joint velocity sets to each of the other sets. This can be expressed as

$$[{}_1 G_\phi^u] {}_1 \dot{\phi} = [{}_r G_\phi^u] {}_r \dot{\phi}, \quad (r=2, 3, \dots, R). \quad (7)$$

The linear relations of Eq. (7) can be rearranged and regrouped according to the independent coordinate velocity set $\dot{\phi}_a$ and the dependent coordinate velocity set $\dot{\phi}_p$ as

$$\dot{\phi}_p = [G_a^p] \dot{\phi}_a. \quad (8)$$

Eq. (8) shows the first-order IKIC (internal kinematic influence coefficient) matrix of the given closed system. And a relationship between the total joints and the independent joints is obtained as

$$\dot{\phi} = [G_a^\phi] \dot{\phi}_a \quad (9)$$

where

$$[G_a^\phi] = \begin{bmatrix} [I] \\ [G_a^p] \end{bmatrix}. \quad (10)$$

Since the joints of the r^{th} chain (${}_r \phi$) are composed of some of the independent and dependent joints, ${}_r \dot{\phi}$ can be expressed in terms of independent joints of the total system by

$${}_r \dot{\phi} = [{}_r G_a^\phi] \dot{\phi}_a, \quad (11)$$

where an augmented matrix $[{}_r G_a^\phi]$ is obtained from $[G_a^p]$ by properly arranging of the independent and dependent joints in the r^{th} chain. Thus, the forward kinematics for the common object space is obtained by embedding the first-order IKIC into one of the pseudo open-chain kinematic expression as follows;

$$\dot{u} = [{}_r G_\phi^u] \dot{\phi}_r = [G_a^u] \dot{\phi}_a, \quad (12)$$

where the forward Jacobian is determined by

$$\begin{bmatrix} G_a^u \end{bmatrix} = \begin{bmatrix} r G_\phi^u \end{bmatrix} \begin{bmatrix} r G_a^\phi \end{bmatrix}. \quad (13)$$

By the same augmentation method employed in Eq. (12), the second-order forward kinematics in terms of independent joints can be easily obtained as

$$\ddot{u} = \begin{bmatrix} G_a^u \end{bmatrix} \ddot{\phi}_a + \dot{\phi}_a^T \begin{bmatrix} H_{aa}^u \end{bmatrix} \dot{\phi}_a. \quad (14)$$

C. General Stiffness Modeling

In a state of static equilibrium among actuator torques, gravity loads at links, and externally applied loads, the system tends to oscillate like a spring once the system is perturbed from its equilibrium state. Yi and Freeman [13] introduced a general stiffness model for general closed-chain mechanism driven by abundant number of actuators.

However, we need to modify the previous stiffness model for passive hands-on devices, which do not take any motor action to control of the oscillatory motion of the system, but employ counter weight instead. In such systems, analysis of the open-loop stability is significant and thus the stiffness model will be used as a means to analyze the open-loop stability of the system.

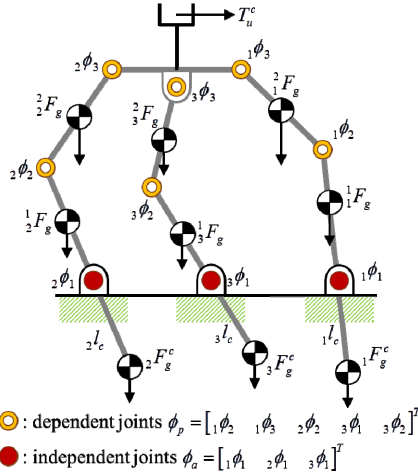


Figure 2. Multi-Loop Mechanism.

The system dynamics of general closed-chain systems can be represented in terms of a minimum(independent) coordinate set equal in number to the minimum number of inputs required to completely describe the system kinematics (see Fig. 2). The system's effective torque T_a^* , felt at a set of "independent" joints ϕ_a , is described in terms of the system's effort sources (T_a and T_p), the effective gravity loads (T_ϕ^G), externally applied loads or upper counter-balance loads ($T_u^{c\text{upper}}$) at the operation space, and lower counter-balance loads ($T_u^{c\text{lower}}$) at the joint space as follows

$$T_a^* = T_a + \begin{bmatrix} G_a^p \end{bmatrix}^T T_p + \begin{bmatrix} G_a^\phi \end{bmatrix}^T T_\phi^G + \begin{bmatrix} G_a^u \end{bmatrix}^T F_u^{c\text{upper}} + T_a^{c\text{lower}} \quad (15)$$

where

$$\begin{cases} T_\phi^G = \begin{bmatrix} {}^1T_\phi^G & {}^2T_\phi^G & \cdots & {}^RT_\phi^G \end{bmatrix}^T, \\ {}^jT_\phi^G = \sum_{i=1}^{M_j} \begin{bmatrix} {}^iG_\phi^c \end{bmatrix}^T {}^iF_g, \quad (j=1, 2, \dots, R) \end{cases} \quad (16)$$

$$\begin{cases} T_a^{c\text{lower}} = \begin{bmatrix} G_a^{c\text{lower}} \end{bmatrix} F_g^{c\text{lower}}, \\ \begin{bmatrix} G_a^{c\text{lower}} \end{bmatrix} = \begin{bmatrix} {}^1l_c \cos {}^1\phi_a & & & 0 \\ & {}^2l_c \cos {}^2\phi_a & & \\ & & \ddots & \\ 0 & & & {}^jl_c \cos {}^j\phi_a \end{bmatrix}, \\ F_g^{c\text{lower}} = \begin{bmatrix} {}^1f_g^{c\text{lower}} & {}^2f_g^{c\text{lower}} & \cdots & {}^jf_g^{c\text{lower}} \end{bmatrix}, \quad (j=1, 2, \dots, R) \end{cases} \quad (17)$$

iF_g : gravity load at the i -th link of the j -th chain

$F_g^{c\text{lower}}$: counter weight at three base joints

l_c : moment arm at the base joint of the first chain

An effective restoring force $\Delta(T_a^*)$ is generated against external disturbances, and its behavior can be modeled as a spring action with respect to the system's "independent" inputs (ϕ_a) as follows

$$\Delta(T_a^*) = -\begin{bmatrix} K_{aa}^* \end{bmatrix} \Delta\phi_a, \quad (18)$$

where the total system stiffness $\begin{bmatrix} K_{aa}^* \end{bmatrix}$ for the independent system inputs and is defined as

$$\begin{aligned} \begin{bmatrix} K_{aa}^* \end{bmatrix} &= -\frac{\partial T_a^*}{\partial \phi_a} \\ &= \begin{bmatrix} K_{aa}^F \end{bmatrix} + \begin{bmatrix} G_a^p \end{bmatrix}^T \begin{bmatrix} K_{pp}^F \end{bmatrix} \begin{bmatrix} G_a^p \end{bmatrix} + \\ &\quad (-T_p)^T \begin{bmatrix} H_{aa}^p \end{bmatrix} + \\ &\quad (-T_\phi^G)^T \begin{bmatrix} H_{aa}^\phi \end{bmatrix}^T + \begin{bmatrix} G_a^u \end{bmatrix}^T \begin{bmatrix} V \end{bmatrix} \begin{bmatrix} G_a^\phi \end{bmatrix} + \\ &\quad (-F_u^{c\text{upper}})^T \begin{bmatrix} H_{aa}^u \end{bmatrix} + \\ &\quad (-F_a^{c\text{lower}})^T \begin{bmatrix} H_{aa}^{c\text{lower}} \end{bmatrix} \end{aligned} \quad (19)$$

where

$$\begin{cases} \begin{bmatrix} V \end{bmatrix} = \begin{bmatrix} I \end{bmatrix} \begin{bmatrix} B_1 & B_2 & \cdots & B_j \end{bmatrix}^T, \\ \begin{bmatrix} B_j \end{bmatrix} = \sum_{i=1}^M ({}^iF_g)^T \begin{bmatrix} {}^iH_{\phi\phi}^c \end{bmatrix}, \quad (j=1, 2, \dots, R) \end{cases} \quad (20)$$

In (19), the first row includes the feedback stiffness matrix (or passive stiffness) at the independent/dependent joints and the second row is the stiffness matrix due to antagonistically fighting actuator torques [13]. These components in the first and second rows will not appear in the passive hands-on devices. The third row corresponds to the stiffness matrix due to the gravity loads of links and the upper platform. The fourth and fifth rows correspond to the stiffness due to upper counter-balancing and lower counter-balancing, respectively.

In our problem, only the components of the third, fourth, fifth rows will remain. The positive definiteness of the effective stiffness matrix will describe the open-loop stability of the system.

III. OPEN-LOOP STABILITY ANALYSIS

A. Exemplary Parallel Mechanism

The open-loop stability is analyzed with one exemplary parallel mechanism having translational three degrees of freedom. Fig. 3 shows a well-known three degree-of-freedom translational mechanism [15]. Three identical limbs connect the moving platform to the stationary platform. Each limb consists of an upper arm (planar four-bar parallelogram) and a lower arm.

We consider three methods of counter-balancing (see Fig. 3). The first method is based on the operational space where the top platform is pulled upward as shown in Fig. 4(a) to balance the gravity loads of links (It will be called “upper counter-balancing”), the second method is based on the joint space where a counter-weight is hanged at the extended-end of proximal links as shown in Fig. 4(b) (It will be called “lower counter-balancing”), and the third method is combing both methods (It will be called “antagonistic counter-balancing”) as shown in Fig. 4(c). The stiffness matrix associated with each case is written below each figure.

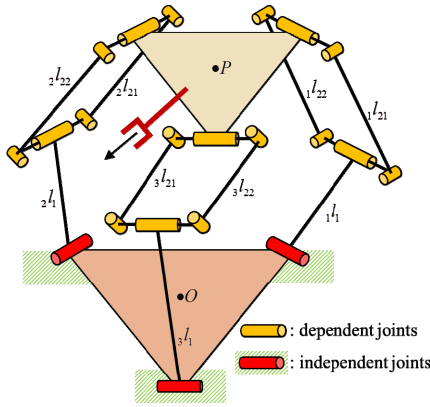
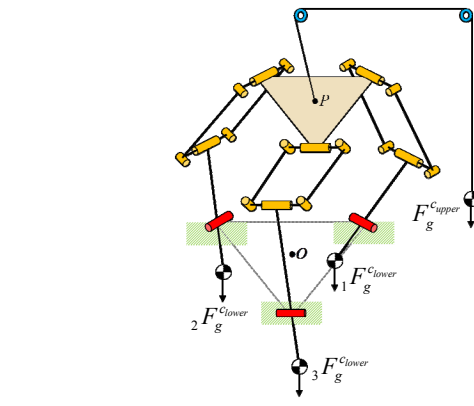
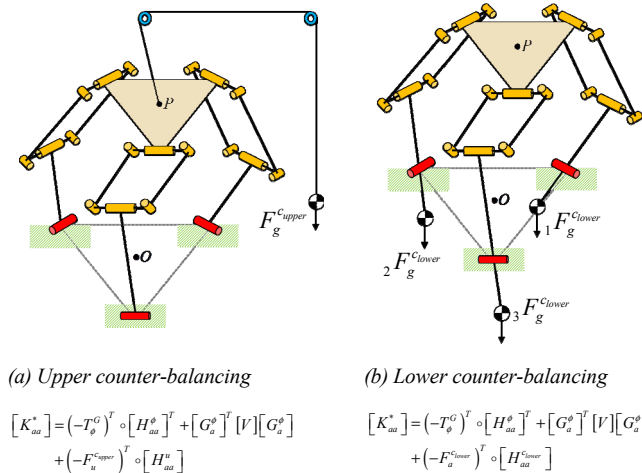


Figure 3. Three degree-of-freedom translational mechanism.



(c) Antagonistic counter-balancing (combination of (a) and (b))

$$[K_{aa}^*] = (-T_p^o)^T \circ [H_{aa}^o]^T + [G_a^o]^T [V] [G_a^o] + (-F_u^{c_upper})^T \circ [H_{aa}^u] + (-F_u^{c_lower})^T \circ [H_{aa}^{c_lower}]$$

Figure 4. Methods of counter-balancing.

B. Open-loop Stability Analysis

As a measure of the open-loop stability, we employ the determinant of the stiffness matrix (i.e., product of eigenvalues for the stiffness matrix). Table 1 includes the simulation parameters. Fig. 5, Fig. 6, and Fig. 7 show the simulation results of the open-loop stability analysis of the three counter-balancing methods. In the Z direction, the lower counter-balancing method is relatively stable ($\det[K] > 0$ and closer to zero) as compared to the other cases (see Fig. 5). However, in the X and Y directions, the lower counter-balancing method is unstable ($\det[K] < 0$) (see Figs. 6 and 7). On the other hand, the upper counter-balancing method is stable in all directions. However, the magnitude of the determinant is fairly large, which implies a large restoring force toward the equilibrium position. Intuitively, a small restoring force is desirable for the system to be used as a passive hands-on device.

As a compromise of the lower and upper counter-balancing methods, we combine the two approaches as shown in Fig. 4(c). As a result, the determinant is always positive and its magnitude is relatively smaller. Thus, we adopt this antagonistic counter-balancing method to design a passive hands-on device.

TABLE I. SIMULATION PARAMETERS

Link Parameters	Dynamic Parameters
$j_1 l_1 = 120 \text{ mm}$	Mass of $j_1 = 0.349 \text{ kg}$
$j_2 l_2 = 150 \text{ mm}$	Mass of $j_2 = 0.183 \text{ kg}$
Radius of the upper plate $r_t = 70 \text{ mm}$	Mass of the upper plate = 1.969 kg
Radius of the lower plate $r_b = 100 \text{ mm}$	Mass of the upper counter-weight $M_{upper} = 1.446 \text{ kg}$
	Mass of the lower counter-weight $j M_{lower} = 1.446 \text{ kg} (j = 1, 2, 3)$

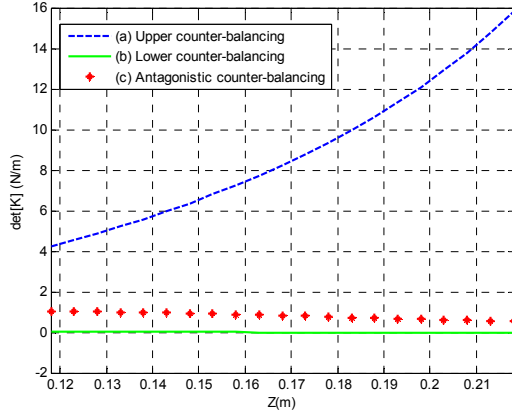


Figure 5. Simulation result of the open-loop stability analysis in the Z direction.

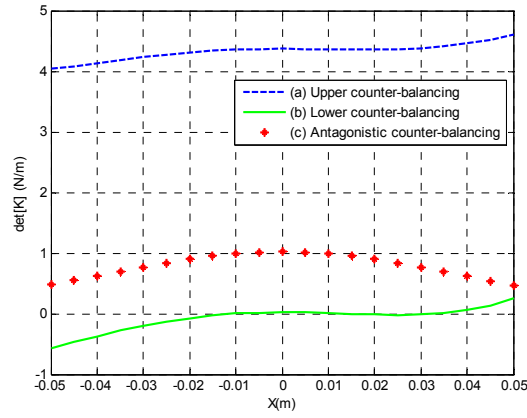


Figure 6. Simulation result of the open-loop stability analysis in the X direction.

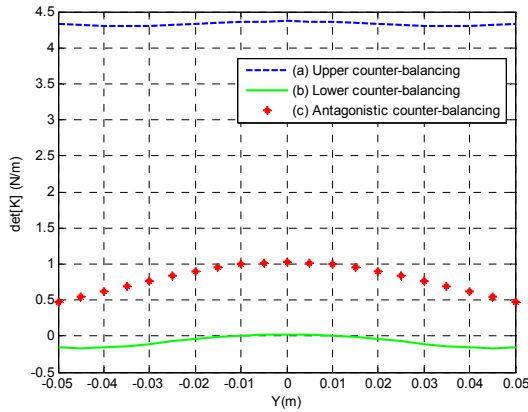


Figure 7. Simulation result of the open-loop stability analysis in the Y direction.

C. Adjustable Moment Arm

The antagonistic counter-balancing was found to have the best open-loop stability. However, still a small restoring force exists in the neighborhood of the equilibrium position upon perturbation. So, in order to ensure the open-loop stability and minimize the restoring force throughout the workspace, an adjustable moment arm is designed at base joints where

counter-weights are installed as shown in Fig. 8. In other words, the moment arm at base joints is calculated and its length is adjusted such that a static equilibrium can be sustained at every position. Conclusively, the upper counter-weight is fixed (passive), but the lower counter-weight is actively adjusted by changing the moment arm of the counter weight. A small motor was employed to change the length of the moment arm.

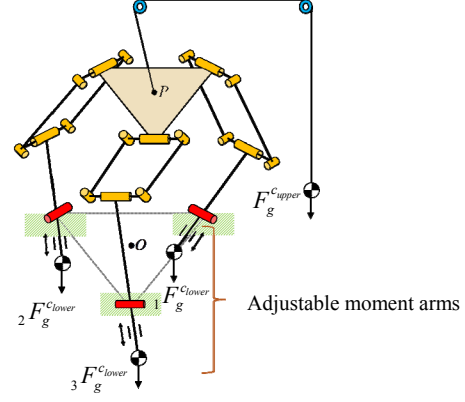


Figure 8. Adjustable moment arm model.

IV. EXPERIMENTAL RESULT

We developed a 3-DOF translational mechanism as shown in Fig. 9. This mechanism consists of a 3-DOF translational parallel mechanism, an upper counter-weight connected by some pulleys and wire, the three lower counter-weights located at three base joints, the adjustable links for minimizing restoring force, a hands-on tool, and three encoders at three base joints for forward kinematics.

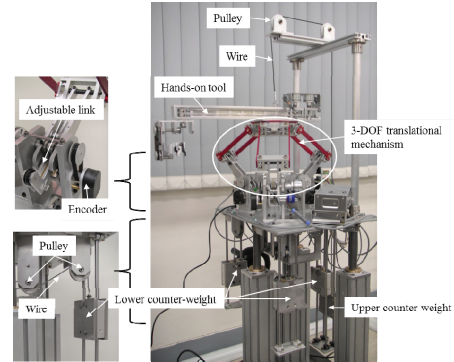
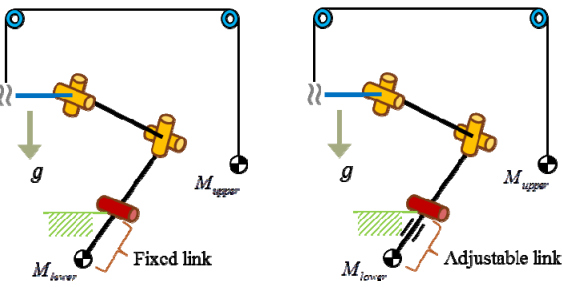


Figure 9. 3 DOF parallel mechanism.

Initially, we set the center location of the mechanism as the equilibrium position and pull the hand-on tool to the X and Y direction, respectively. And then we measured the restoring forces. Fig. 10 denotes a simplified model of the Fig. 4(c) and Fig. 8. Fig. 11 shows the test environment for the force measurement. A force sensor is mounted at a platform in the left-side and a wire connects the hands-on device to the force sensor. Pulling the hands-on device to the X or Y direction, a restoring force is measured. Table II denotes the measured force data in the X direction. It is easily noted that Case I corresponding to the fixed link yields some restoring force but that Case II corresponding to the adjustable link does not feel any restoring force along the pulled direction owing to

changing its equilibrium position continuously. Zero restoring force in Case II implies that the system is perfectly counter-balanced. Thus, the operator does not feel any force when he pulls the hands-on device in any direction. Thus, he is able to handle the end-tool as in the free space without paying any effort.



(a) Case I : with the fixed link (b) Case II : with the adjustable link

Figure 10. Comparison of two models.

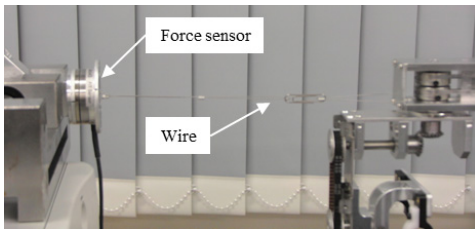


Figure 11. Test environment to measure the restoring force

TABLE II. FORCE MEASUREMENT RESULT IN THE X DIRECTION

	Distance (mm)	20	30	40
Case I	Force (N)	0.7	1.3	1.8
Case II	Force (N)	0.0	0.0	0.0

The video clips attached to this paper include the following contents.

- (i) A multi-body dynamic simulator (“DAFUL” made of Virtual Motion Co. [16]) is employed to simulate the open-loop stability of three counter-balancing methods
- (ii) Demonstration of the restoring force for the fixed link
- (iii) Demonstration of the zero restoring force for the adjustable link.

V. CONCLUSION

Need for counter-balancing mechanism is expected to grow much specially in the area of passive hands-on devices. In such case, analysis of the open-loop stability is very important. The major contribution of this paper is the inclusion of a general stiffness model and a measure to analyze the open-loop stability. Through both dynamic simulation and experiment, we demonstrated the effect of the open-loop stability.

Such a passive hands-on device with full counter-balancing introduced in this paper can be beneficially employed for minimally invasive Otologic surgery. Otologic surgery requires high manipulation speed just like the surgeon’s

operation and safeguard for small critical organs such as facial nerves since they are located under the bone. An image-guided Otologic surgery based on such a passive hands-on device is our ongoing research topic.

ACKNOWLEDGEMENTS

This work is supported by the Technology Innovation Program (10040097) funded by the Ministry of Trade, Industry and Energy Republic of Korea (MOTIE, Korea), supported by GRRC program of Gyeonggi Province (GRRC HANYANG 2013-A02), and financially supported by the Ministry of Trade, Industry and Energy (MOTIE) and Korea Institute for Advancement in Technology (KIAT) through the Workforce Development Program in Strategic Technology, supported by the MOTIE(The Ministry of Trade, Industry and Energy), Korea, under the Robotics-Specialized Education Consortium for Graduates support program supervised by the NIPA(National IT Industry Promotion Agency) (H1502-13-1001)

REFERENCES

- [1] T. Laliberte, C.M. Gosselin, and M. Jeam, "Static balancing of 3-DOF planar parallel mechanisms," *IEEE/ASME Tran. on Mechatronics*, vol. 4, no. 4, pp. 363-377, December 1999.
- [2] J. Wang and C.M. Gosselin, "Static balancing of spatial three-degree-of-freedom parallel mechanisms," *Mechanism and Machine Theory*, vol. 34, pp. 437-452, 1999.
- [3] C.M. Gosselin and J. Wang, "Static balancing of spatial six-degree-of-freedom parallel mechanisms with revolutive actuators," *Journal of Robotic Systems*, vol. 17, no. 3, pp. 159-170, 2000.
- [4] A.M. Tahmasebi, B. Taati, F. Mobasser, and K. Hashtrudi-Zaad, "Dynamic parameter identification and analysis of a PHANToM™ haptic device," in *Proc. of IEEE Conf. on Control Applications*, pp. 1251-1256, August 2005.
- [5] A. Agrawal and S.K. Agrawal, "Design of gravity balancing leg Orthosis using non-zero free length springs," *Mechanism and Machine Theory*, vol. 40, 6, pp. 693-709, June 2005.
- [6] K. Nakamura, M. Dol, T. Hashimoto, and M. Nakamura, "Holding arm apparatus for medical tool," U.S. Patent 0162476 A1, July 7, 2011.
- [7] K. Nakamura, "Biaxial balance adjusting structure for medical stand apparatus," U.S. Patent 5 480 114, January 2, 1996.
- [8] K. Nakamura, M. Dol, and M. Nakamura, "Medical stand apparatus," U.S. Patent 6 045 104, April 4, 2000.
- [9] K. Nakamura and T. Ota, "Balancing char," U.S. Patent 5 927 815, July 27, 1999.
- [10] S. Lessard, P. Bigras, and I. A. Bonev, "A new medical parallel robot and its static balancing optimization," *ASME Trans. J. Med. Devices*, vol. 1, no. 4, pp. 272-278, October 2007.
- [11] J.-J. Park, Y.-J. Lee, J.-B. Song, and H.-S Kim, "Safe joint mechanism based on nonlinear stiffness for safe human-robot collision," in *Proc. of IEEE Int. Conf. on Robotics and Automation*, pp. 2177-2182, May 2008.
- [12] B.-J. Yi, I. D. Walker, D. Tesar, and R.A. Freeman, "Geometric stability in force control," in *Proc. of IEEE Int. Conf. on Robotics and Automation*, pp. 281-286, April 1991.
- [13] B.-J. Yi, and R.A. Freeman, "Geometric analysis of antagonistic stiffness in redundantly actuated parallel mechanisms," *Journal of Field Robotics*, vol. 10, no. 5, pp. 581-603, July 1993.
- [14] R.A. Freeman and D. Tesar, "Dynamic modeling of serial and parallel mechanisms/robotic systems, Part I : Methodology, Part II : Applications," in *Proc. of 20th ASME Mech. Conf.*, vol. 15-3, pp. 7-27, 1988.
- [15] L.-W. Tsai, G.C. Walsh, and R.E. Stamper, "Kinematics of a novel three DOF translational platform," in *Proc. of IEEE Int. Conf. on Robotics and Automation*, pp. 3446-3451, April 1996.
- [16] www.virtualmotion.co.kr